Turbulent drag reduction by bio-polymers in large scale pipes

Marina Campolo[*]

Department of Chemistry, Physics and Environment

University of Udine

Udine, 33100, Italy

Email: marina.campolo@uniud.it

Mattia Simeoni

Department of Elec., Manag., and Mechanical Engineering

University of Udine

Udine, 33100, Italy

Email: mattia.simeoni@uniud.it

Romano Lapasin

Department of Engineering and Architecture

University of Trieste

Trieste, 34128, Italy

Email: romano.lapasin@di3.units.it

Alfredo Soldati [†]

Department of Elec., Manag., and Mechanical Engineering

University of Udine

Udine, 33100, Italy

Email: alfredo.soldati@uniud.it

ABSTRACT

In this work we describe drag reduction experiments performed in a large diameter pipe (i.d. 100 mm) using a semi-rigid bio-polymer (Xanthan Gum, XG). The objective is to build a self consistent data base which can be used for validation purposes. To this aim, we run a series of tests measuring friction factor at different XG

---

[*]Corresponding author

[†]also at Centro Internazionale di Scienze Meccaniche, CISM, 33100 Udine, Italy

concentrations (0.01, 0.05, 0.075, 0.1 and 0.2% w/w XG) and at different values of Reynolds number (from 758 to 297,000). For each concentration, we obtain also the rheological characterization of the test fluid. Our data are in excellent agreement with data collected in a different industrial scale test rig. Data are used to validate design equations available from the literature. Our data compare well with data gathered in small scale rigs and scaled up using empirically based design equations and with data collected for pipes having other than round cross section. Our data confirm the validity of a design equation inferred from Direct Numerical Simulation which was recently proposed to predict the friction factor. We show that scaling procedures based on this last equation can assist the design of piping systems in which polymer drag reduction can be exploited in a cost effective way.

1   Introduction

The use of polymer additives is common in civil and process engineering and in many food, pharmaceutical and biomedical processes (see [1] and references therein). When added to a turbulent flow, polymers are subject to local flow conditions and undergo tumbling, flow orientation, chain stretching and relaxation. The net effect of all these conformational changes appears as an intrinsic elastic stress which alters the flow field [2] and the dynamics of near wall turbulent structures which control the momentum transfer to the wall. The macroscopic result is a dramatic reduction of the friction factor. Such drag reduction has been exploited for flood control in sewer system, firefighting systems, dredging operations, drilling applications and for the improved transport of suspended solids (see [3]). For those applications in which the long term accumulation of the polymer in the receiving "environment" or the contamination of the (solvent) fluid are issues of concern, bio-polymers are used instead of traditional synthetic polymers since they can be bio-degraded more easily.

Despite the variety of potential applications, guidelines to design large scale systems are still lacking: homogeneous sources of experimental data collected in large size pipes are limited and design is based on empirical correlations fitted on data collected in small scale pipes with inevitable uncertainties in the use of such correlations at industrial scale. In recent years, complementary theory has been proposed to describe the mechanisms responsible for drag reduction (see the review by [4]) and numerical experiments have been performed to examine the implications of the theory and how they compare with reality: Direct Numerical Simulations (DNS) of turbulent drag reduction by polymers elucidated the role of viscosity profile [5], polymer relaxation time [6], polymer elasticity [7], effective wall viscosity [8], and of the dynamic interaction between polymer and vortices ([2, 9] among others) on the redistribution of turbulent energy in the wall layer which induces the drag reduction. The main advantage of numerical experiments is that the effect of polymer properties (such as elasticity, stretching and concentration), domain geometry and flow conditions can be more easily isolated and studied. Nevertheless, the correctness/adequacy of the underlying physical model needs to be corroborated *a-posteriori* by independent experimental data [9]. Recently Housiadas and Beris [10], building on the systematic analysis of their DNS database, proposed a parametric relationship to predict friction factors in viscoelastic turbulent flows. This relationship could be potentially used to assist the design of piping systems exploiting polymer induced drag reduction.

The object of this work is to build a self consistent data set investigating turbulent drag reduction in large pipes (100 mm i.d.) with the final aim of validating the new theoretical correlation. We focus on a semi-rigid bio-polymer, Xanthan Gum (XG), used as flow enhancer both in process and food industry, running a series of tests to measure drag reduction of aqueous solutions of the polymer at different concentrations (0.01, 0.05, 0.075, 0.1 and 0.2% w/w XG). Specifically, for each XG concentration, we measure the steady state shear viscosity and friction factor in a wide range of Reynolds numbers

(from 758 to 297,000). We validate our data set against data gathered at the same scale by [11]. We evaluate and discuss the predictive ability of one empirical scaling [12] based on drag reduction data collected in laboratory scale test rigs (pipe diameter equal to 3, 5 and 6 mm, in [13]; 10, 25 and 50 mm in [14]; 2, 5, 10, 20 and 52 mm in [15]). We evaluate also changes in drag reduction expected when pipes with different cross section are used based on drag reduction data obtained for pipes with rectangular and annular cross sections [16–18]. We use our data to corroborate the relationship proposed in [10] demonstrating the capability of that model to scale up (or scale down) our drag reduction data to any larger (smaller) scale of interest. Finally, we explore the potential practical use of the correlation for the cost-effective optimization of industrial systems.

2   Methodology

2.1   Flow Loop

The flow loop used for the experiments (already described in [19]) is sketched in Fig. 1. A 3.0 m^3 capacity tank is used to feed the flow to a centrifugal pump (CALPEDA NM 65/16 AE, maximum flow rate 120 m^3/h) delivering the fluid through the loop; the loop consists of two branches of straight, smooth pipe (each 14 m long) placed one above the other ($\Delta H = 2.4\ m$) and connected by a semicircular bend of large radius. The loop is about 35 m long overall (350 D). At the end of the loop, the fluid is collected by a receiving tank and recirculates back by gravity to the feeding tank. The fluid flow rate can be varied in the range $10 \div 81\ m^3/h$ changing the frequency of the inverter (SILCOVERT SVTSplus, AsiRobicon) which controls the pump.

In this work, the measuring section is limited to the last portion of the lower branch of the rig (140 D long), enclosed by the dashed rectangle in Fig. 1. A general purpose resistance thermocouple (K type) is placed upstream the measuring section and is used to monitor the fluid temperature (accuracy $\pm 1^o C$). A Yokogawa electromagnetic flow-meter (model SE200ME/NE, span 100 m^3/h, accuracy 0.5% of span for $U = [0.3 \div 1\ m/s]$, 0.25% of span for $U > 1\ m/s$) is used to measure flow rate data. High quality pressure tap holes (2 mm diameter), carefully machined to avoid viscoelastic hole pressure errors, are present at 4 positions along the measuring section (ports A, B, C and D, interdistance equal to 3 m); they are connected with 6 mm internal diameter clear vinyl tubing to a capacitive differential pressure transmitter (MHDS by Müller Industrie Elektronik). The accuracy on pressure drop measured by the transducer is estimated to be higher than 0.1 mbar (0.075% of Full Scale, 120 mbar). Fluid temperature was manually recorded for each flow rate acquisition and at the beginning and at the end of each test run. In house software was written (National Instrument Labview) to record flow rate and pressure drop readings during the tests.

As shown in Fig. 1, a small stirred tank (200 L capacity, stirred by Protool MXP1202 E EF, 150-360 RPM, 1200 W, equipped with a triple spiral HS3R impeller) is provided to prepare a concentrated master solution of polymer powder and solvent (tap water). The solution is prepared according to instructions of the product data sheet, i.e. adding carefully the powder to well stirred water and continuing stirring until a smooth, clear solution is obtained. The last step to prepare the test solution is diluting the master solution with additional water to reach the desired polymer concentration inside the feeding tank. Final homogenization of the polymer solution in the tank is obtained by circulating the fluid through the short return loop (3 m length overall).

For viscoelastic fluids the entry length can be significantly larger than for a Newtonian fluid in both laminar [20] and turbulent flow conditions [21]. Therefore, a number of preliminary tests was performed to identify the best pair of pressure

ports to be used to collect accurate measurements of differential pressure readings. The objective of these tests, performed using tap water and 0.2% XG solution as test fluids, was threefold: (i) verify that, for each fluid, the flow was fully developed in the measuring section in the range of Reynolds number tested (i.e. the specific pressure drop was independent from location and inter-distance of pressure taps); (ii) choose the pair of pressure taps for which the error on differential pressure can be minimized; (iii) gather data for the reference pressure drop measured along the pipe when pure solvent is flowing. Tests results showed that difference in pressure loss per unit length of pipe measured using ports B-C and B-D for both water and 0.2% XG was less than 1%, indicating fully developed flow in the measurement section. Pressure taps B and D were finally selected to measure pressure loss to maximize the accuracy of $\Delta P/L$ values. Ports B and D are 6 m apart (60 D), with tap B 6 m (60 D) downstream the flow meter and tap D 1 m (10 D) upstream the inlet of the return bend.

2.2 Test Fluid Characterization

The fluids used in the present work are aqueous solutions of Xanthan Gum, a pharmaceutical grade supplied by CP-Kelco (commercial name Xantural 75). The complete rheological characterization of the XG solutions should be based on continuous shear experiments to evaluate shear viscosity and first normal stress difference [1, 22], oscillatory shear experiments to evaluate storage and loss moduli [23], extensional flow tests to evaluate extensional viscosity [17] and dynamic light scattering analysis to highlight any change in the polymer chain conformation as a function of concentration, temperature and solvent type [24]. Such a complete rheological characterization is beyond the scope of this work and we decided to focus only on a subset of relevant rheological quantities. As discussed by [10], the minimal set of parameters required to develop predictive correlations includes the viscosity of the solution at the wall and a time scale (polymer relaxation time) representative of the response of the polymer under extensional deformation encountered in turbulent flows. Therefore, we performed steady state shear viscosity tests to define a rheological constitutive equation predicting fluid viscosity at the wall, and we decided to rely on the *a-posteriori* evaluation of an effective polymer relaxation time directly from drag reduction data.

The steady shear viscosity of the test fluids was determined using a stress controlled rheometer (Haake RS150) equipped with cone and plate geometry ($C60/1^o$). Temperature control of the solution during testing was done using a refrigerated water bath (Thermo/Haake F6). Each test for the rheological characterization of the fluid was performed according to the following procedure: a mild shear condition (constant shear rate $100 \ s^{-1}$, corresponding to shear stress values in the range $0.1 \div 3.7 \ Pa$, maintained for 120 s) was imposed to the sample to cancel any effect of the previous rheological history and followed by a stepwise sequence of ascending shear stress values (10 per decade and logarithmically spaced in the range $0.02 \div 20 \ Pa$). The duration of each constant stress segment was 90 s or shorter if the steady state response of the fluid was attained or approached with a preset approximation. The wide shear rate interval explored in the experimental tests covers quite different structural conditions, ranging from an almost unperturbed polymer configuration to stretched and oriented chain conformations, expected when the fluid is circulated inside the experimental loop.

Figure 2 shows the results of rheological tests performed at $T = 20^oC$ for the characterization of the five polymeric solutions. Additional measurements were made also at 15^oC and 25^oC (not shown). Figure 2 (a) shows shear stress versus shear rate measured by the rheometer for the various XG solutions (solid symbols). The solid line represents the linear relationship between shear stress and shear rate for tap water, our reference Newtonian fluid. The range of shear stress values investigated is wider than that expected for water moving at different flow rates inside the experimental loop, shown by the dashed horizontal lines labelled as Min and Max $\tau_{w,water}$. Figure 2 (b) shows viscosity variation versus shear rate.

The Carreau-Yasuda constitutive equation [25] was used to fit the data corresponding to each polymer concentration:

$$\frac{\eta - \eta_\infty}{\eta_0 - \eta_\infty} = \frac{1}{[1 + (\lambda\dot{\gamma})^a]^{n/a}} \tag{1}$$

In Eqn. 1, η is the shear viscosity, η_0 and η_∞ are viscosity at the zero-shear and infinite-shear plateaus while λ, n and a represent the inverse shear rate at the onset of shear thinning, the power law index and the parameter introduced by [25]. Table 1 summarizes the values of fitting parameters evaluated using the methodology outlined in [26]. The corresponding curves are shown as dotted lines on the graph.

Figure 2 (b) shows also the rheological characterization of two 0.2% XG solutions: the former (Kelco Division of Merck and Co.) used by [11] to perform drag reduction experiments in their 100 mm diameter pipe and the latter (Keltrol TF, Kelco Division of Merck and Co.) used by [17] to perform drag reduction experiments in an annular pipe. Both curves, drawn based on the values of the fitting parameters reported in Tab. 1, indicate that large deviations can exist between viscosity values measured for nominally identical XG solutions. Since we will compare directly our drag reduction data with those of [11], we believe important to assess how large these differences can be. The relative difference between our and [11] viscosity data indicates up to 20% overestimation in the low shear rate range and up to 15% underestimation in the high shear rate range. Our shear viscosity data are 30% lower than those by [17] in the low shear rate range to 20% lower in the high shear rate range.

We processed further our rheological data to derive a model equation predicting viscosity variation for XG solutions as a function of both polymer concentration and shear rate. Details are given in Appendix A.

2.3 Evaluation of Drag Reduction: Testing Protocol

We gathered differential pressure and flow rate data for a number of different flow rates (from 10 to 81 m^3/h for tap water) increasing stepwise the frequency of the inverter in the range 13-50 Hz (step 2 Hz). After each change of inverter frequency, we monitored in time the flow rate variation to identify the length of the transient necessary to reach steady state conditions inside the flow loop (about 5 min at the smaller flow rate and about 1 min at the larger flow rates). From this time on, we sampled data for a time period of 2 minutes (data acquisition rate of 5 Hz). Statistics calculated from sampled data were used to (i) identify average values of $Q, \Delta P$ pairs and to (ii) check variability of test conditions during each steady state. During each steady state, the standard deviation of flow rate data was comparable with the accuracy of the flow meter (± 0.5 m^3/h) for both tap water and XG solutions. The standard deviation of the pressure signal was found to increase proportionally with the flow rate, ranging within [$0.8 \div 8$ $mbar$] for tap water and dilute XG solution (XG <0.10%); the standard deviation of the pressure signal was found to be almost independent of the flow rate ([$0.5 \div 0.6$ $mbar$]) for the more concentrated 0.2% XG solution.

Tests were performed in triples to assess their repeatability over time. Average values of $Q, \Delta P$ gathered over the three tests were then compared to identify deviations due to other effects, such as temperature changes or ageing of polymer solution. We observed no systematic change of ΔP over the three tests (generally performed within three subsequent days), indicating no significant mechanical degradation of the polymer during testing; whereas, since we did not used biocides, we observed the spontaneous development of microbial activity in concentrated solutions after the fourth day of storage when environmental temperature was above 20^oC.

3 Results

3.1 Velocity and Specific Pressure Drop

Figure 3 shows average values of specific pressure drop, i.e. pressure drop per unit length, $\Delta P/L$, versus section averaged bulk velocity, $U = 4Q/\pi D^2$, calculated from measurements made in the flow loop. Each point represents the average over three tests, while errorbars identify data variability among the three tests performed. Considering the repeatability of each test, the accuracy of flow rate measurements was estimated to be better than $\pm 2.5\%$ whereas the accuracy of pressure drop measurements was estimated to be better than $\pm 4\%$. Maximum variability of pressure drop was larger ($\pm 10\%$) for tests performed using 0.075% XG solution.

Empty circles represent the specific pressure drop measured for tap water. The solid line corresponds to the value of the specific pressure drop calculated assuming that the pipe is hydraulically smooth. In such condition, the friction factor can be calculated as

$$f = \frac{16}{Re}, \text{ if } Re \leq 2100 \tag{2}$$

$$\frac{1}{\sqrt{f}} = 1.7 \cdot \ln(Re\sqrt{f}) - 0.4, \text{ if } Re > 2100 \tag{3}$$

Equation 3 is known as the von Kármán equation. The agreement between experimental data and the calculated values of specific pressure drop is excellent, confirming the proper calibration of the experimental set up.

The specific pressure drop measured for XG solutions is shown by solid symbols. The arrow indicates increasing XG concentration. For velocity values in the range $U = [0.35 \div 1 \ m/s]$, the measured value of specific pressure drop is about the same as in tap water for most of the aqueous XG solutions. A different behavior is observed only for the largest concentration tested, 0.2% XG, where the measured specific pressure drop is larger than for tap water. Drag enhancement at large polymer concentration and small Reynolds number has been already observed for rigid polymers [27,28] and attributed to the homogeneous increase of effective viscosity of the fluid which prevails over the reduction of momentum flux to the wall. At larger Reynolds number, i.e. for velocity values in the range $U = [1 \div 3 \ m/s]$, the measured specific pressure drop for XG solutions is always less than in tap water. The largest reduction in specific pressure drop is found at the largest concentration of XG.

3.2 Comparison Against Literature Data

3.2.1 Same geometrical scale [11]

We compared friction factor data measured for our 0.2% XG concentration solution with those measured by [11] in a rig of the same diameter. To this aim, we calculated the Fanning friction factor, f,

$$f = \frac{2\tau_w}{\rho U^2} \quad \text{with} \quad \tau_w = \frac{\Delta P}{L}\frac{D}{4} \tag{4}$$

and the generalized Reynolds number, $Re = Re_{MR}$, for a shear-thinning fluid defined as $Re_{MR} = \rho U D/\eta^*$ where ρ is the fluid density, U is the average velocity, D is the internal diameter of the pipe and η^* is the effective viscosity of the fluid. This definition of the Reynolds number is equivalent to the generalized Reynolds number defined by [29] for laminar flow, and is still meaningful for turbulent flow [30]. The effective viscosity is evaluated as $\eta^* = \eta(3n_{pl} + 1)/4n_{pl}$ where η is the apparent viscosity corresponding to the pressure drop measurement (see Eqn. 4) in the Carreau-Yasuda model fit to the steady-shear

viscosity measurements; the second factor is the Weissemberg-Rabinowitsch correction where n_{pl} is the (local) power law index of the fluid (also evaluated from the rheological data). Using this definition, Eqn. 2 represents the reference curve to fit friction factors calculated for Newtonian and non Newtonian fluid in the laminar region. In the rest of the paper, we will use indifferently Re or Re_{MR} to refer to the generalized Reynolds number.

Figure 4 shows the variation of the friction factor versus Reynolds number for the different aqueous solutions of XG tested. Considering the repeatability of each test and the accuracy of flow rate and pressure drop measurements, we estimated maximum experimental uncertainties up to $\pm 2.5\%$ for the generalized Reynolds number and up to $\pm 9\%$ for the friction factor. The curve corresponding to the friction factor for laminar/turbulent flow in a smooth pipe calculated using Eqn. 2 and 3 is shown as a solid line; the maximum drag reduction (MDR) asymptote found by Virk [31], given by

$$\frac{1}{\sqrt{f}} = 8.2515 \cdot \ln(Re\sqrt{f}) - 32.4 \tag{5}$$

is shown as a dotted line. The experimental data obtained by [11] (XG 0.2%, open triangle pointing upward) are also shown for comparison.

Consider first our data (solid symbols only). For each value of the Reynolds number, the friction factor calculated for XG solutions is always smaller than for tap water (solid line); the difference between friction factors of XG solution and tap water increases with polymer concentration. The difference does not significantly change as the Reynolds number increases, indicating a Type-B behavior (rigid, rod-like chain) for XG (see [15]). For XG 0.2% and in the small flow rate region ($\simeq 10\ m^3/h$, corresponding to $Re_{MR} \simeq 1000$, i.e. in the laminar regime), the values of the friction factor for the polymeric solution align along the laminar curve and to the Virk MDR asymptote.

Comparison between our data obtained for XG 0.2% (solid triangle pointing upward) with those by [11] (open triangle pointing upward) indicates very good agreement: deviations are within $\pm 7\%$ for $Re_{MR} < 4,000$ and decrease down to 2% at larger Reynolds numbers.

3.2.2 Scale Up of Drag Reduction Data from Smaller Diameter Pipes

Similarly to other polymers, also for XG solution drag reduction was measured many times in small diameter pipes [13, 15, 32]. In this work, we tried to scale up data available from the literature to the size of our pipe. After a review, we selected the data by [13] as a candidate data set to test the accuracy of scaling laws available from the literature. Experiments were performed in three different pipes ($D_1 = 3.146\ mm$, $D_2 = 5.186\ mm$ and $D_3 = 6.067\ mm$) using two commercial XGs (Flocon 4800C by Pfizer in tap water and Rhodopol 23 by Rhone-Poulenc in distilled water added with 100 ppm NaCl) for 0.01%, 0.1% and 0.2% XG concentrated solutions. Polymer additive, values of concentration and type of solvent are similar to our experiments, whereas pipe diameters are much smaller.

The difficulty of scaling up such data was early pointed out by [33], among others. They defined %DR as

$$\%DR = 100 \cdot \left.\frac{\Delta P_w - \Delta P_p}{\Delta P_w}\right|_{Q=const} = \%DR_Q \tag{6}$$

where ΔP_w and ΔP_p are the pressure drop measured for the Newtonian fluid (water) and for the polymer added fluid flowing, at the same flow rate Q, along the pipe. They found that %DR data measured for specific polymeric solutions flowing in pipes of different size and plotted versus pipe diameter depend on the pipe size: for small pipes, %DR can be very high,

reaching the Virk MDR asymptote; for larger pipes, %DR moves away from the MDR asymptote, decreasing as the diameter increases and eventually reaching a plateau when the pipe diameter is large enough (order 10^2 for Guar Gum and order 10^3 *mm* for Hydropur SB125 from their data). This "pipe diameter effect" actually prevents the direct use of data collected at the small scale, $D_1 \simeq O(10^1)$ *mm*, to infer the drag reduction expected at the larger scale, $D_0 \simeq O(10^2 \div 10^3)$ *mm*. As a result, a number of design equations have been proposed to scale up DR data (see [14] and more recently [15, 34] among others).

We followed the work of [14] and subsequent works by [35] and used the "negative roughness" approach to scale the small diameter data (D_1, D_2 and D_3) to our pipe dimension (D_0). The methodology is based on the assumption of similarity between velocity profiles in pipes of different size, which is generally satisfied unless the size of the experimental pipe becomes too small. In such case, the similarity of velocity profiles is broken because of the growing extension of the viscous sub-layer (see [12]). In Bewersdorff's data base [13], pipe diameters are 20 to 30 times smaller than our pipe and this might make the scaling inaccurate [12].

The scaling is based on two equations which allows to transform the Prandtl-Kármán (P-K) coordinates corresponding to data obtained for pipe dimension D_i to P-K coordinates corresponding to data obtained for pipe dimension D_0. Equations are the following:

$$(Re\sqrt{f})_0 = (Re\sqrt{f})_i \cdot \left(\frac{D_0}{D_i} \right) \tag{7}$$

to translate the x-coordinate, and

$$\frac{1}{\sqrt{f}} = 1.7 \ln \left(\frac{Re\sqrt{f}}{4.67} + N \right) + 2.28 \tag{8}$$

to translate the y-coordinate. Equation 7 states that, to make meaningful comparison between scale D_i and D_0, the shear stress (and the shear velocity) should be the same in the two geometries. This produces the same level of conformational change (uncoiling/stretching and/or preferential orientation) of the polymers (and the same rheological behavior for the testing fluid) in the small and in the large pipe. Equation 8 is the analogous of Colebrook equation [36] including a negative roughness parameter $N = D/k$, where k is the dimensional "negative roughness". It is used twice: the first time to calculate the value of the negative roughness N using the pair of $(Re\sqrt{f}, 1/\sqrt{f})$ values known at scale D_i, and the second time to evaluate $1/\sqrt{f}$ at scale D_0.

Figure 5 shows original data from [13] (gray symbols), rescaled data (open symbols) and our data (solid symbols). Diamonds refer to 0.01% XG whereas circles to 0.10% XG. Solid and dotted lines represent data for tap water and Virk [31] MDR asymptote as in previous graphs. We should remark here that we did not considered for scaling those original data which lay in the MDR region. Therefore, we disregarded the entire 0.2% XG concentration data set of [13] and some points from the other two data sets.

Compared to original data (gray symbols), rescaled data (open symbols) matching the equivalent shear rate condition in the larger pipe are shifted upward and to the right (as indicated by the dashed arrow). For 0.01% XG (Rhodopol 23 with 100 ppm NaCl) (diamonds), the agreement between our data and rescaled data by [13] is quite good even if type A drag reduction (i.e. different slope of polymer solution and solvent data) is observed for that data set whereas type B drag reduction (i.e. same slope of polymer solution and solvent data) is observed for our data set. The difference in $1/\sqrt{f}$ is less than 3% for

$Re\sqrt{f} < 10^4$ and $4 \div 7\%$ for $Re\sqrt{f} > 10^4$. This corresponds to deviation in the friction factor in the range $7 \div 12\%$. Deviation are most likely due to the different concentration of NaCl in the two testing fluids (100 ppm in [13], versus $\simeq 50\ ppm$ in our tap water), resulting in a different flexibility of the polymer (see [15]).

Data shown in [13] for 0.1% XGs (circles) correspond to the two different XGs tested: Rhodopol 23 with 100 ppm NaCl for full gray symbol and Flocon 4800 C in tap water for white and gray symbol. As apparent from the plot, after rescaling to diameter D_0 data collected in pipe D_1 and D_2 exhibit type B and type A drag reduction, respectively. Only a qualitative comparison is possible between rescaled data and our data since they span a different range of $Re\sqrt{f}$. However, rescaled data corresponding to the Flocon in tap water data set seem to align with our data along one single line parallel to the Kármán line.

3.2.3 Effect of Pipe Cross Section

We compared our drag reduction data with data available for acqueous solutions of XG in rectangular and annular pipes [16–18] to check if any systematic difference exists in drag reduction due to the shape of the pipe. This information may be useful for design purposes since in many industrial devices (e.g. heat exchangers, air conditioning systems), circular pipes are not the typical choice and drag reduction is still a crucial issue.

Escudier [16] (ENP in Fig. 6) evaluated drag reduction in a rectangular pipe (height $H = 25\ mm$, width $W = 298\ mm$, hydraulic diameter $D_{H1} = 46\ mm$ and aspect ratio $W/H = 11.92$) for flow rates up to $90\ m^3/h$. The aspect ratio of their pipe was large enough to hypothesize strong 2D flow in the cross section. The Xanthan Gum was Keltrol TF, supplied by Kelco Ltd, and was tested at 5 different concentrations (0.03, 0.05, 0.067, 0.08 and 0.15% w/w XG). Data selected for comparison are from the 0.05% XG data set: points are far from the MDR asymptote and the concentration is one of those we tested. Original data, available in the form of (Re, f) pairs (with the Reynolds number $Re = HDU/2\nu$ defined based on the channel half-height) were converted into (Re_H, f) pairs (with $Re_H = 4Re$ defined based on the hydraulic diameter) and rescaled using Eqn. 7 and 8.

Jafar [17, 18] (JP in Fig. 6) evaluated drag reduction in an annular pipe ($D_{inner} = 50.8\ mm$, $D_{outer} = 100\ mm$, hydraulic diameter $D_{H2} = 49.2\ mm$) and flow rates up to $90\ m^3/h$. The Xanthan Gum was Keltrol TF, supplied by Kelco Ltd, and was tested at 3 different concentrations (0.0124, 0.07 and 0.15% w/w XG). Data selected for comparison are from the 0.0124 and 0.07% XG data sets: points are far from the MDR asymptote and the concentrations are similar to the ones tested. Original data available in the form of Reynolds number (based on hydraulic diameter) and friction factor were rescaled using Eqn. 7 and 8.

Figure 6 shows the comparison between data obtained for the rectangular (ENP) and the annular (JP) geometry and present results. Diamonds, squares and triangles correspond to 0.01% XG, 0.05% XG and 0.075% XG concentrations, respectively. Our data are shown as solid symbols, original JP/ENP data are shown as gray symbols and rescaled JP/ENP data are shown as open symbols. The values of hydraulic diameters ($D_{H0} = 100\ mm$, circular pipe, $D_{H1} = 46\ mm$ for the rectangular pipe and $D_{H2} = 49.2\ mm$ for the annular pipe) corresponding to each geometry are also indicated.

Despite the very different shapes of pipe cross sections used to collect the friction factor data, the comparison indicates a quite good agreement: for the annular section, deviation between JP and our friction factors is about $7 \div 8\%$ for 0.01% XG, whereas there is an almost perfect agreement (error less than 2%) for 0.075 % XG. For the rectangular section, the error on the friction factor is 5% at maximum.

3.3 Assessment of Predictive Correlation by Housiadas and Beris [10]

We used our data to assess the correlation developed by [10] to predict the friction factor in viscoelastic turbulent pipe flow. According to their model, the visco-elastic response of a polymer solution is described by a universal drag reduction curve in which the Weissemberg number, defined as the ratio of the polymer relaxation time to the time scale of turbulence at the wall, $We_\tau = \lambda^* u_\tau^2 / \nu$ is the independent parameter. $We_\tau \simeq O(1)$ ($We_\tau \simeq 6$ from DNS results) identifies the onset of drag reduction whereas for large enough values of We_τ the DR levels up to a limiting value (Limiting Drag Reduction, LDR).

The correlation is therefore based on two dimensionless parameters: (i) the zero shear-rate elasticity parameter, El_0, defined as $El_0 = \lambda^* \nu_0 / R^2$ where λ^* is a scale for the polymer relaxation time, $\nu_0 = \eta_0/\rho$ is the kinematic zero shear-rate viscosity of the solution and R is pipe radius; and (ii) the Limiting Drag Reduction, LDR, i.e. the drag reduction observed at high Weissemberg numbers. The predictive equation can be written as:

$$\frac{1}{\sqrt{f}} = \frac{1}{(1-DR)^{\tilde{n}/2}} \cdot$$

$$\left(1.7678 \cdot \ln(Re\sqrt{f}) - 0.60 - \frac{162.3}{Re\sqrt{f}} + \frac{1586}{Re^2 f} \right) \tag{9}$$

where DR is the drag reduction produced by the polymer in any specific flow conditions and $\tilde{n}$ is a coefficient which is a weak function of Re.

In Fig. 7 we show the percent drag reduction calculated from our data according to the definition given by [10]:

$$\%DR_\tau = \left[1 - \left(\frac{Re^{(visc)}}{Re^{(Newt)}} \right)^{-2/\tilde{n}}_{Re_\tau} \right] = 100 \cdot DR \tag{10}$$

where the bulk Reynolds number for the viscous and the Newtonian fluid are evaluated at the same value of friction Reynolds number (shown along the x-axis). From the plateau of $\%DR_\tau$ shown in Fig. 7 we estimated the value of LDR, which is different for each polymer concentration. We used the value of Re_τ corresponding to the onset of drag reduction for the 0.2%XG concentration data set (identified by the open triangle) to calculate the zero shear rate elasticity value ($El_0 = 0.087$) and the time scale for the polymer relaxation ($\lambda^* = 0.20\,s$ for 0.2%XG). Oscillatory shear stress tests performed by [1] on salt free solutions of XG in the range of concentration $200 \div 2000\,ppm$ indicate an almost constant value of the polymer relaxation time ($\simeq 10\,s$) [1]. This value is quite different from the relaxation time of the model λ^* confirming the inherent difficulty already underlined by [10] in linking the polymer relaxation time scale of the model with data derived from rheological tests. Given the difficulty of estimating an indipendent value of El_0 for each XG concentration from our experimental data (the onset is not defined for $XG \neq 0.2\%$) we decided to use the same value of the fitting parameter El_0 whichever the XG concentration. Values of the dimensionless parameters used in the correlation are summarized in Tab. 2.

In Fig. 8 we show our experimental data together with the prediction obtained from the correlation (dashed lines) (see Appendix B for details on model equations) using P-K coordinates. The agreement between our data and the correlation is very good: maximum deviation is 3.5% for 0.1%XG at $Re_{MR}\sqrt{f} \simeq 700$.

3.4 Scale Up and Scale Down of Friction Factor Data Using Experimentally Fitted Predictive Correlation

In Fig. 9 we show how the correlation by [10] can be used to predict the value of friction factor in pipes of different size ($D = 0.005, 0.25, 0.5$ and 1 m) for a given viscoelastic fluid (0.2%XG solution in our example). The two key dimensionless

parameters, *LDR* and El_0, fitted from our experimental data, are modified as follows for scaling purposes: we keep fixed the value of LDR, since it depends only on polymer concentration; for each pipe diameter D, we rescale the zero shear rate elasticity value $El_0 = 0.087$ calculated from our experimental data (corresponding to $D_0 = 0.1$ *m*), as $El_0(D) = El_0(D_0) \cdot (D_0/D)^2$.

The elasticity parameter controls the onset of drag reduction (the higher El_0 the earlier the onset) and increases as the pipe size is reduced [10]. Two main effects are apparent from the analysis of Fig. 9: (i) the value of friction Reynolds number at onset of drag reduction increases with pipe diameter; (ii) the MDR asynthote is early reached in small pipe diameters.

Housiadas and Beris [10] remark the difficulty in obtaining precise values for λ^* (and therefore El_0) *a-priori* based on the rheological characterization of the fluid. It is also clear that information about the scale for polymer relaxation time can not be derived from tests performed in small pipe diameter, where the onset Re_τ can be well below the minimum friction Reynolds number for which tests can run. The scaling shown in Fig. 9 suggests that experiments performed at intermediate scales (larger than the laboratory scale and yet not as large as the typical industrial applications) could be profitably used to derive the two key parameters (i.e. the time scale for the polymer relaxation and the limiting value of drag reduction) necessary to scale-up (or scale-down) friction factor data to any other scale of interest.

4 Cost-Effective Use of Drag Reducing Agents

4.1 Drag Reduction

In industrial practice, the effectiveness of a polymer as drag reducing agent (DRA) is described by the drag reduction level, %DR, which is a function of the friction factor. Many different definitions of drag reduction have been used in the literature (see Eqn. 6, 10 and 11). All of them are related and can be calculated from (Re, f) pairs available from experiments. In this work, we choose to define drag reduction as the change in pressure drop (or wall shear stress) due to the presence of the polymer to the original Newtonian value, while keeping the same mean flow rate [37, 38] (see Eqn. 6). This definition states clearly the link between the industrial target, i.e. the transport of a given amount of fluid along a pipeline, and the benefit possibly produced by drag reduction, i.e. energy savings due to a smaller pressure loss. When the density and viscosity of the polymeric solution do not change significantly with the polymer addition, our definition is equivalent to

$$\%DR_{Re} = \frac{f_w - f_p}{f_w}\bigg|_{Re=const} \cdot 100 \tag{11}$$

where the difference in friction factors is evaluated keeping the Reynolds number constant [8, 16].

Figure 10 shows *%DR_Q* evaluated by Eqn. 6 as a function of bulk velocity, U (as in [34]). Since experimental measurements of pressure drop for XG solution and water are not available at the same flow rate, Eqn. 2 and 3 are used to calculate the friction factor of the tap water flowing at the same flow rate (and velocity) of the polymer solution. For 0.01% XG solution, the drag reduction is almost constant in the entire range of velocities investigated. For any XG concentration greater than 0.01%, the profile of *%DR_Q* increases with bulk velocity, eventually reaching a plateau. Figure 10 (b) shows the maximum value of *%DR_Q*, *%DR_max*, obtained for each XG concentration. Similarly to the analysis presented by [39] for Polyox, *%DR_max* increases with XG concentration, but less than proportionally to the amount of polymer added, C. Figure 10 (a) shows also that, for any XG concentration greater than 0.01%, we can identify a threshold value of bulk velocity in the pipe, U_t, above which drag reduction is produced (i.e. *%DR_Q* > 0). Since the polymer is semi-rigid, this threshold velocity should not be associated with a coiled/stretched transition. Rather, it should be considered as an indicator of the

level of Newtonian shear rate above which the conformational change is such that the homogeneous increase in the effective viscosity is counterbalanced by the reduction of momentum flux to the wall in the near wall layer [27, 28]. Figure 10 (c) shows the value of U_t, interpolated/extrapolated from data in Fig. 10 (a) and labelled with letters. The threshold bulk velocity seems to increase almost linearly with polymer concentration (dashed line in Fig. 10 (c)) in the range of values investigated. These results are consistent with Direct Numerical Simulations [6] which indicate that the onset of drag reduction is observed when the Weissemberg number exceeds a (constant) threshold value. Considering that λ^* depends primarily on molecular characteristics [10], the onset condition corresponds to increasing values of friction, u_τ and bulk velocity, U, for increasing concentration of XG in solution (and larger ν).

Figure 10 (c) indicates that, if we consider a reference bulk velocity equal to 1 m/s as the target for the economical transport of fluid along pipelines, the addition of XG at any concentration (among those tested) lower than 0.2% will produce some drag reduction. According to Fig. 10 (a), the %DR expected by 0.05% XG, 0.075% or 0.1% XG is about the same at this velocity. The effect the relative amount of polymer added has on %DR is best appreciated when the fluid velocity increases up to $2 \div 3 \, m/s$ (i.e. at larger Re numbers, moving into the LDR region).

4.2 Cost-Effectiveness Analysis

Figure 11 (a) shows isocontours of *%DR* (dotted lines, step 2%, starting from zero to 46%, labelled in gray) obtained from our tests. Similar data could be obtained for pipes of different diameter using the design equation discussed in Section 3.4. Isocontours are drawn for velocity in the range $U = [0 \div 3 \, m/s]$ and $\%XG = [0 \div 0.2]$. We do not extend *%DR* isocontours in the lower left region of the graph ($U < 0.35 \, m/s$ and $C < 0.01\%XG$), since we have no experimental data there. In the top left corner region (high concentration, low velocity), the polymer does not produce drag reduction (drag enhancement region). At large enough velocity (i.e. into the LDR region), drag reduction becomes almost independent of velocity and increases with polymer concentration.

Isocontours of *%DR* alone are not enough to evaluate if the use of the drag reducing polymer may represent a cost-effective alternative for the transport of fluid along a piping system. Our evaluation will be based on a cost-effectiveness analysis which builds up on the following assumptions: (i) the piping system is already installed (initial investment costs for pump and pipe equipments are neglected); (ii) the concentrated pressure drop due to bends, elbows, fittings and valves has been adequately represented as distributed pressure drop generated by (properly defined) equivalent pipe lengths; (iii) mechanical degradation of the polymer during the transport of fluid has negligible effect on pressure drop. These represent conservative assumptions for the identification of threshold operative conditions in which the polymer addition can be considered cost effective. The operating costs we are supposed to pay to convey the fluid are (i) the pumping costs and (ii) the polymer additive cost and can be conveniently referred to the unit of mass of fluid to be conveyed. We define the percent net savings, %S, as:

$$\%S = 100 \cdot \frac{C_w - C_p}{C_w} [\%]$$

(12)

where C_p and C_w are transport costs per unit mass with/without the DRA. C_w can be calculated as the product of the price of energy times power and working hours divided by the mass of fluid conveyed:

$$C_w = \frac{K_E \Delta P_w Q N_h}{\rho Q N_h} \quad [\text{€/kg}]$$

(13)

where K_E is the price of energy, [€/kWh], ΔP_w is the pressure loss, [Pa], Q is the flow rate, [m^3/h], N_h is the number of pump working hours, [h], and ρ is fluid density, [kg/m^3]. C_p can be calculated as the product of the price of energy times power and working hours plus the price per unit mass of polymer times the mass of polymer, divided by the mass of fluid conveyed:

$$C_p = \frac{K_E \Delta P_p Q N_h + K_P \cdot \%XG\rho Q N_h}{\rho Q N_h} \tag{14}$$

where ΔP_p is the pressure loss with the DRA, [Pa], $\%XG$ is the concentration (w/w) of DRA, [kg_p/kg], K_P is the price of DRA per unit mass, [€/kg_p]. Considering that $\Delta P_p = (1 - \%DR_Q)\Delta P_w$ (from Eqn. 6) and $\Delta P_w = 2f_w L\rho U^2/D$, Eqn. 12 becomes:

$$\%S = \%DR_Q - \frac{K_P}{K_E}\frac{\%XG}{2f_w U^2 L/D} = \%DR_Q - \frac{1}{\alpha}\frac{\%XG}{2f_w U^2} \quad [\%] \tag{15}$$

where $\alpha = K_E/K_P \cdot L/D \ [s^2/m^2]$ or [kg/J] is a dimensional factor which depends on the prices (of energy and polymer) and on pipeline characteristics (L/D). In short, $\%S = F(U, \%XG, \alpha)$. The use of the DRA is cost-effective only if $\%S > 0$. The largest is the value of $\%S$, the most cost-effective is the use of the polymer.

In Fig. 11 (a)-(d) we show positive isocontours of $\%S$ (continuous lines, colored online, step 2%, starting from zero). The color scale (from red, bottom to pale blue, top) identifies increasing values of $\%S$. Subfigures (a)-(d) show the variation of $\%S$ isocontours calculated for different values of the parameter α.

Values of α may be associated with different values of energy/polymer price ratio or with pipelines characterized by a different L/D ratio. In this work, we assume the price of energy is $K_E = 0.15$ €/kWh, the price of polymer is $K_P = 10$ €/kg, and pipe size is $D = 0.1 \ m$. The values of α considered in Fig. 11 correspond to pipeline 120, 240, 600 and 1200 km long (values comparable with ductworks in small to large cities).

Figure 11 can be used to identify if the polymer addiction represents a cost-effective solution for a given pipeline scenario or not. Assume that the task is to transport fluid at $U = 2 \ m/s$ along the pipeline. In the scenario shown in Fig. 11 (a), the most cost effective option, identified by the circle, is to use no polymer. Even if drag reduction up to 38% can be achieved using 0.2%XG, this would not produce net savings because the polymer cost would be larger than savings obtained in pumping cost. In the scenario shown in Fig. 11 (b), i.e. a bit longer pipeline or a different economical scenario in which the price of energy is larger and savings on pumping costs can be more significant, the most cost effective option would be to add polymer at small concentration (e.g. 0.03%XG) to obtain about 18% drag reduction and 7% net savings. In the third scenario, shown in Fig. 11 (c), the most cost effective option would be to add polymer at larger concentration (e.g. $\simeq 0.1\%$XG) to obtain up to 32% drag reduction and more significant net savings (about 20%). Finally, in the fourth scenario, shown in Fig. 11 (d), the most cost effective option would be to add a bit more polymer (concentration about 0.125%XG) to obtain up to 26% net savings.

5   Conclusions

In this work, we build a self-consistent data base measuring ΔP versus Q for different aqueous solutions of XG (Xantural 75 at 0.01, 0.05, 0.075, 0.1 and 0.2% w/w XG) in an industrial size rig (100 mm i.d.). The data set includes the rheological characterization of aqueous XG solutions used for testing and drag reduction data measured at different Reynolds number (from 758 to 297,000) for five XG concentrations (in the dilute and semi-dilute polymer concentration region). The data

set, representing a homogeneous source of experimental data gathered on a large pipe, has been used for the validation of existing predictive correlations.

We validated our experiments by direct comparison with data by [11] who performed experiments at the same scale, in the same pipe geometry. Deviations are 4-7% and are most likely associated with non constant properties of the different XGs commercially available. We assessed also the possibility of scaling up drag reduction data from experiments performed at a smaller scale or on different pipe geometries. Drag reduction data collected in laboratory scale rigs [13] and scaled up to the larger scale of our test rig shows deviation of the friction factor in the range $7 \div 12\%$. Drag reduction data collected in pipe with rectangular [16] or annular [17, 18] cross sections shows deviation in the range $7 \div 8\%$. We used our data to confirm the validity of the design equation proposed by [10], demonstrating also the capability of their model to scale up (or scale down) our drag reduction data to any larger (smaller) scale of interest. By the cost-effectiveness analysis proposed at the end of the paper we identify sets of working conditions for the profitable use of XG polymer as DRA. We show that, for each industrial scenario, the most cost-effective option for the use of XG should be identified based on the joint analysis of (i) %DR data evaluated at different bulk velocity and for solutions at different %XG concentration and of (ii) the value of the cost parameter α, combining data on energy/polymer prices with the specific pipeline characteristics.

A   Model Equation to Predict Viscosity of XG Solutions

Figure 12 (a) shows the log-log plot of zero-shear viscosity versus concentration obtained for our data (solid circles) and for XG data available from the literature (open triangles, data from [17]; open circle, data from [11]). The two solid lines represent power law equations of the type $\eta_0(C) = K_H \cdot C^{n'}$ fitting the experimental data in the dilute (smaller slope) and semi-dilute (larger slope) polymer concentration region. Present data indicate a critical overlap concentration at about 0.05%, which is in agreement with data found in the literature (0.067% in [17]; 0.08% in [1]). Values of fitting parameters are $K_H = 0.066$ and $n' = 0.8446$ in the dilute region and $K_H = 1073.83$, $n' = 4.08$ in the semi-dilute region. According to [17], $\eta_0 \propto C^{1.56}$ and $\propto C^{4.66}$ in the dilute and semi-dilute region. According to [1], $\eta_0 \propto C^{2.0}$ and $\propto C^{4.67}$ in the dilute and semi-dilute region.

Figure 12 (b) shows the variation of viscosity versus XG concentration calculated from the Carreau-Yasuda model fit to our experimental data. Symbols represent different values of shear rate whereas each solid line is a power law fit made only for points at constant shear rate in the semi-dilute range of polymer concentration. For clarity of presentation, only values of shear rate in the range $[10^{-1} \div 10^4]$ are shown. For each value of shear rate, the fitting equation can be written as $\eta(C, \dot{\gamma}) = K'_H(\dot{\gamma}) \cdot C^{n''(\dot{\gamma})}$. This equation can be used to predict changes in viscosity as a function of shear rate and XG concentration if the functional relationships $K'_H(\dot{\gamma})$ and $n''(\dot{\gamma})$ are known. Figure 12 (c) summarizes the value of parameters $K'_H(\dot{\gamma})$ and $n''(\dot{\gamma})$ derived from the fitting procedure. This graph can be used to estimate the viscosity of XG solutions for which the direct rheological characterization is not available.

B   Housiadas and Beris [10] Predictive Correlation

The input dimensionless parameters to derive the values of $(Re\sqrt{f}, 1/\sqrt{f})$ pairs shown in Fig. 8 are El_0 and LDR whereas We_τ is the independent variable. For each value of We_τ, we use (1) the universal fitting curve and the value of LDR

to calculate the drag reduction, DR:

$$\frac{DR}{LDR}(We_\tau) = \begin{cases} 0 & \text{if } We_\tau < We_\tau^{onset} \\ 1 - \dfrac{2}{1+\exp\left(\frac{We_\tau - We_\tau^{onset}}{\Delta We_\tau}\right)} & \text{if } We_\tau \geq We_\tau^{onset} \end{cases}$$

and (2) the rheological constitutive equation to calculate the wall dynamic viscosity normalized to the zero shear rate viscosity:

$$\mu_w = \frac{\eta}{\eta_0} = \frac{\eta_\infty}{\eta_0} + \left(1 - \frac{\eta_\infty}{\eta_0}\right) \frac{1}{[1 + (\Omega \cdot We_\tau)^a]^{n/a}} \tag{16}$$

where $\Omega \cdot We_\tau = \gamma\lambda$ and $\Omega = \lambda/\lambda^*$. The value of μ_w is used (3) to calculate the zero shear rate value of Weissemberg number, $We_{\tau,0} = We_\tau \cdot \mu_w$, (4) the zero shear rate friction Reynolds number ($Re_{\tau,0} = \rho u_\tau R/\eta_0$) from El_0:

$$Re_{\tau,0} = \left(\frac{We_{\tau,0}}{El_0}\right)^{1/2} \tag{17}$$

and (5) the friction Reynolds number, $Re_\tau = Re_{\tau,0}/\mu_w$. Then, starting from the initial guess for $\tilde{n} = 1.18$, we calculate (5) the bulk Reynolds number:

$$Re = \frac{2\sqrt{2}Re_\tau}{(1 - DR)^{\tilde{n}/2}} \cdot$$

$$\left(1.7678\ln(2\sqrt{2}Re_\tau) - 0.60 - \frac{162.3}{2\sqrt{2}Re_\tau} + \frac{1586}{2\sqrt{2}Re_\tau}\right) \tag{18}$$

(6) a new value for $\tilde{n}$:

$$\tilde{n} = 1 + \frac{1.085}{\ln Re} + \frac{6.538}{(\ln Re)^2} \tag{19}$$

iterating (5) and (6) up to convergence. Finally, we calculate (7) the friction factor as $f = 8Re_\tau^2/Re^2$. From our experimental data for 0.2%XG, the value of $Re\sqrt{f}$ at the onset of drag reduction (empty triangle in Figure 8) is 142.69, from which we calculate $Re_\tau = 50.44$ and $\mu_w = 0.0269$. Since $We_\tau = 6$ at onset and $El_0 = We_\tau/(Re_\tau^2\mu_w)$, we calculate $El_0 = 0.087$.

C Acknowledgements

References

[1] Wyatt, N. B., and Liberatore, M. W., 2009. "Rheology and viscosity scaling of the polyelectrolyte xanthan gum". *J. Applied Polymer Science,* **114**(6), pp. 4076–4084.

[2] Kim, K., and Sureshkumar, R., 2013. "Spatiotemporal evolution of hairpin eddies, reynolds stress, and polymer torque in polymer drag-reduced turbulent channel flows". *Phys. Rev. E,* **87**(6), p. 063002.

[3] Kamel, A., and Shah, S. N., 2009. "Effects of salinity and temperature on drag reduction characteristics of polymers in straight circular pipes". *J. Petroleum Sci. & Eng.,* **67**(1-2), pp. 23–33.

[4] White, C. M., and Mungal, M. G., 2008. "Mechanics and prediction of turbulent drag reduction with polymer additives". *Annual Rev. Fluid Mech.,* **40**, pp. 235–256.

[5] De Angelis, E., Casciola, C. M., L'vov, V. S., Pomyalov, A., Procaccia, I., and Tiberkevich, V., 2004. "Drag reduction by a linear viscosity profile". *Phy. Rev. E,* **70**(5), p. 055301(R).

[6] Min, T., Jung, Y. Y., Choi, H., and Joseph, D. D., 2003. "Drag reduction by polymer additives in a turbulent channel flow". *J. Fluid Mech.,* **486**, pp. 213–238.

[7] Ptasinski, P. K., Boersma, B. J., Nieuwstadt, F. T. M., Hulsen, M. A., den Brule, V., A., B. H. A., and Hunt, J. C. R., 2003. "Turbulent channel flow near maximum drag reduction: simulations, experiments and mechanisms". *J. Fluid Mech.,* **490**, pp. 251–291.

[8] Housiadas, K. D., and Beris, A. N., 2004. "Characteristic scales and drag reduction evaluation in turbulent channel flow of non constant viscosity viscoelastic fluids". *Phys. Fluids,* **16**(5), pp. 1581–1586.

[9] Dubief, Y., Terrapon, V. E., White, C. M., Shaqfeh, E. S. G., Moin, P., and Lele, S. K., 2005. "New answers on the interaction between polymers and vortices in turbulent flows". *Flow Turb. & Comb.,* **74**(4), pp. 311–329.

[10] Housiadas, K. D., and Beris, A. N., 2013. "On the skin friction coefficient in viscoelastic wall-bounded flows". *Int. J. Heat Fluid Flow,* **42**, pp. 49–67.

[11] Escudier, M. P., Presti, F., and Smith, S., 1999. "Drag reduction in the turbulent pipe flow of polymers". *J. Non Newtonian Fluid Mech.,* **81**(3), pp. 197–213.

[12] Hoyt, J. W., and Sellin, R. H. J., 1993. "Scale effect in polymer pipe flow". *Exp. Fluids,* **15**(1), pp. 70–74.

[13] Bewersdorff, H. W., and Singh, R. P., 1988. "Rheological and drag reduction characteristics of xanthan gum solutions". *Rheologica Acta,* **27**(6), pp. 617–627.

[14] Sellin, R. H. J., and Ollis, M., 1983. "Effect of pipe diameter on polymer drag reduction". *Ind. Eng. Chem. Prod. Res. Dev.,* **22**(3), pp. 445–452.

[15] Gasljevic, K., Aguilar, G., and Matthys, E. F., 2001. "On two distinct types of drag-reducing fluids, diameter scaling, and turbulent profiles". *Non Newtonian Fluid Mech.,* **96**(3), pp. 405–425.

[16] Escudier, M. P., Nickson, A. K., and Poole, R. J., 2009. "Turbulent flow of viscoelastic shear-thinning liquids through a rectangular duct: Quantification of turbulence anisotropy". *J. Non Newtonian Fluid Mech.,* **160**(1), pp. 2–10.

[17] Japper-Jaafar, A., Escudier, M. P., and Poole, R. J., 2010. "Laminar, transitional and turbulent annular flow of drag-reducing polymer solutions". *J. Non Newtonian Fluid Mech.,* **165**(19-20), pp. pp.1357–1372.

[18] Jaafar, A., and Poole, R. J., 2011. "Drag reduction of biopolymer flows". *J. Applied Sciences,* **11**(9), pp. 1544–1551.

[19] Dearing, S. S., Campolo, M., Capone, A., and Soldati, A., 2013. "Phase discrimination and object fitting to measure fibers distribution and orientation in turbulent pipe flows". *Exp. Fluids,* **54**(1), p. 1419.

[20] Poole, R. J., and Ridley, B. S., 2007. "Development-length requirements for fully developed laminar pipe flow of inelastic non-newtonian liquids". *ASME J. Fluids Eng.,* **129**(10), pp. 1281–1287.

[21] Gasljevic, K., Aguilar, G., and Matthys, E. F., 2007. "Measurement of temperature profiles in turbulent pipe flow of polymer and surfactant drag-reducing solutions". *Phys.Fluids,* **19**(8), p. 083105.

[22] Escudier, M. P., and Smith, S., 2001. "Fully developed turbulent flow of non-newtonian liquids through a square duct". *Proc. R. Soc. Lond. A,* **457**, pp. 911–936.

[23] Choppe, E., Puaud, F., Nicolai, T., and Benyahia, L., 2010. "Rheology of xanthan solutions as a function of temperature, concentration and ionic strength". *Carbohydrate Polymers,* **82**(4), pp. 1228–1235.

[24] Rodd, A. B., Dunstan, D. E., and Boger, D. V., 2000. "Characterisation of xanthan gum solutions using dynamic light scattering and rheology". *Carbohydrate Polymers,* **42**(2), pp. 159–174.

[25] Yasuda, K., Armstrong, R. C., and Cohen, R. E., 1981. "Shear flow properties of concentrated solutions of linear and star branched polystyrenes". *Rheol. Acta,* **20**, pp. 163–178.

[26] Escudier, M. P., Gouldson, I. W., Pereira, A. S., Pinho, F. T., and Poole, R. J., 2001. "On the reproducibility of the rheology of shear-thinning liquids". *J. Non Newtonian Fluid Mech.,* **97**(2-3), pp. 99–124.

[27] Amarouchene, Y., Bonn, D., Kellay, H., Lo, T. S., L'vov, V. S., and Procaccia, I., 2008. "Reynolds number dependence of drag reduction by rodlike polymers". *Phys. Fluids,* **20**(6), p. 065108.

[28] Procaccia, I., L'vov, V. S., and Benzi, R., 2008. "Colloquium: Theory of drag reduction by polymers in wall-bounded turbulence". *Rev. Mod. Phys.,* **80**(1), pp. 225–247.

[29] Metzner, A. B., and Reed, J. C., 1955. "Flow of non-newtonian fluids: correlation of the laminar, transition and turbulent flow regions". *AIChE J.,* **1**(4), pp. 434–440.

[30] Chilton, R. A., and Stainsby, R., 1998. "Pressure loss equations for laminar and turbulent non-newtonian pipe flow". *J. Hydraulic.Eng.-ASCE,* **124**(5), pp. 522–529.

[31] Virk, P. S., 1975. "Drag reduction fundamentals". *AIChE J.,* **21**(4), pp. 625–656.

[32] Sasaki, S., 1991. "Drag reduction effect of rod-like polymer solutions. i. influences of polymer concentration and rigidity of skeletal back bone". *J. Physical Society Japan,* **60**(3), pp. 868–878.

[33] Interthal, W., and Wilski, H., 1985. "Drag reduction experiments with very large pipes". *Colloid & Polymer Sci.,* **263**(3), pp. 217–229.

[34] Gasljevic, K., Aguilar, G., and Matthys, E. F., 1999. "An improved diameter scaling correlation for turbulent flow of drag-reducing polymer solutions". *J. Non Newtonian Fluid Mech.,* **84**(2-3), pp. 131–148.

[35] Hoyt, J. W., 1991. "Negative roughness and polymer drag reduction". *Exp. Fluids,* **11**(2-3), pp. 142–146.

[36] Colebrook, C. F., 1939. "Turbulent flow in pipes, with particular reference to the transition region between the smooth and rough pipe laws". *J. Inst. Civil Eng.,* **11**(4), pp. 133–156.

[37] Sharma, R. S., 1981. "Drag reduction by fibers". *Canadian J. Chem. Eng.,* **58**(6), pp. 3–13.

[38] Vlassopoulos, D., and Schowalter, W. R., 1993. "Characterization of the non-newtonian flow behavior of drag-reducing fluids". *J. Non-Newtonian Fluid Mech.,* **49**(2-3), pp. 205–250.

[39] Little, R. C., Hansen, R. J., Hunston, D. L., Kim, O., Patterson, R. L., and Ting, R. Y., 1975. "The drag reduction phenomenon. observed characteristics, improved agents, and proposed mechanisms". *Ind. Eng. Chem., Fundamen.,* **14**(4), pp. 283–296.

Fig.12 Results of rheological data processing: (a) variation of zero-shear viscosity versus concentration; present data (solid circle); ESC (1999) data [11] (open circle); JEP (2010) data [17] (open triangle); power law fitting of data in the dilute and semi-dilute concentration range (solid line, present data; dashed line, JEP data); (b) variation of viscosity versus concentration: symbols identify different values of shear rate, $\dot{\gamma}$, solid lines are power law fit, $\eta = K'_H \cdot C^{n''}$, for concentration values larger than 0.01%; (c) value of fitting parameters K'_H and n'' as a function of shear rate, $\dot{\gamma}$

E   List of Tables

Fig. 1. Experimental flow loop: pipe diameter is 100 mm, loop length is 350 D overall. Measuring section (dashed rectangle) is $140\,D$ long
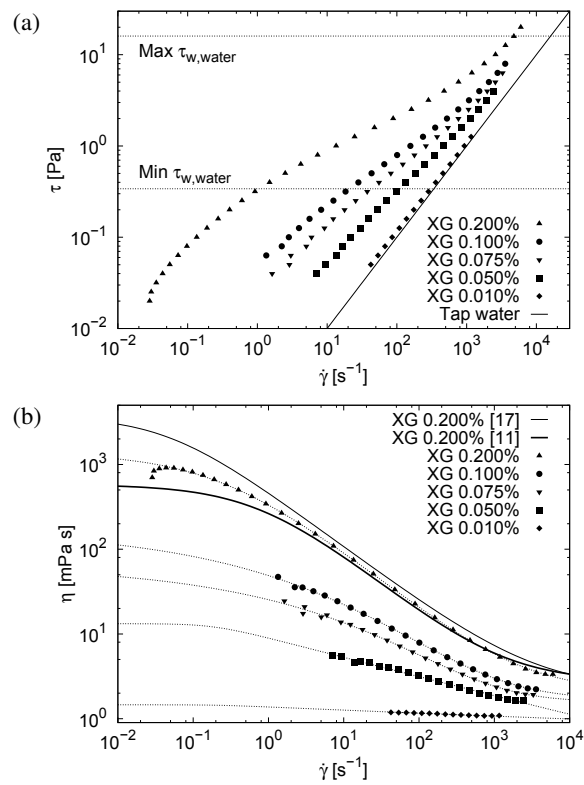
Fig. 2. Results of rheological characterization: (a) shear stress, τ, versus shear rate, $\dot\gamma$ measured in rheometer for various XG concentrations (symbols) and reference curve for water (solid line); shear stress is in the range $[0.02 \div 20\ Pa]$, dashed lines indicate range of variation of shear stress at pipe wall, τ_w in the hydraulic loop; (b) viscosimetric data for various Xanthan Gum concentrations together with the Carreau-Yasuda fits (dotted lines) [25]. Data for XG 0.2% from [11] are shown by a thick solid line. Data for XG 0.2% from [17] are shown by a thin solid line
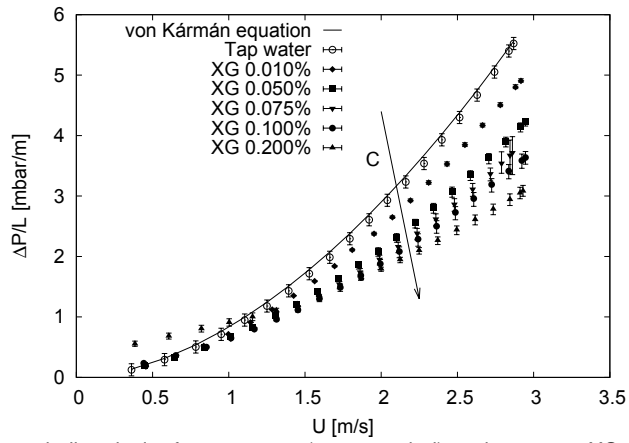
Fig. 3. Specific pressure drop versus bulk velocity for tap water (open symbol) and aqueous XG solutions (solid symbols). Errorbars represent data variability over three independent tests. Solid line is value of specific pressure drop calculated using friction factor given by Eqn. 3. Solid symbols represent different values of XG concentration. The arrow indicates increasing XG concentration
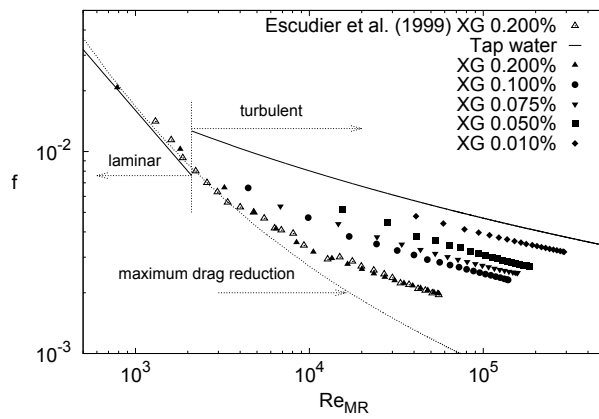
Fig. 4. Comparison against data from [11]: friction factor, f, versus generalized Reynolds number, Re_{MR}; curve for tap water (solid line), maximum drag reduction asymptote (dotted line), data for different XG solutions (solid symbols) and data from [11] (open triangles)
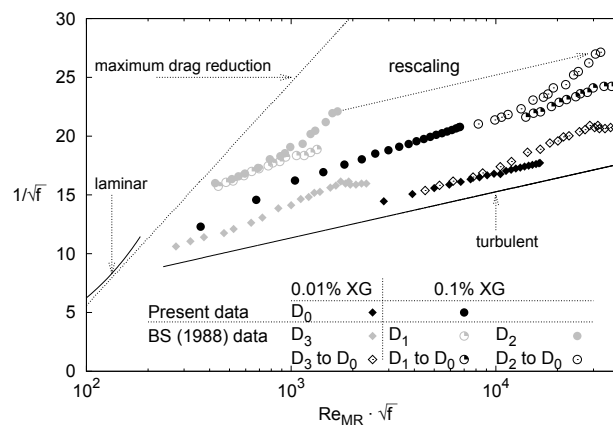
Fig. 5. Comparison against Bewerdorff and Singh (BS) [13] data: 0.01% XG (diamonds), 0.10% XG (circles); present data (solid symbols), original BS data (gray symbols) ($D_1 = 3.146\,mm$, $D_2 = 5.186\,mm$, $D_3 = 6.067\,mm$), BS data rescaled to $D_0 = 100\,mm$ (open symbols)
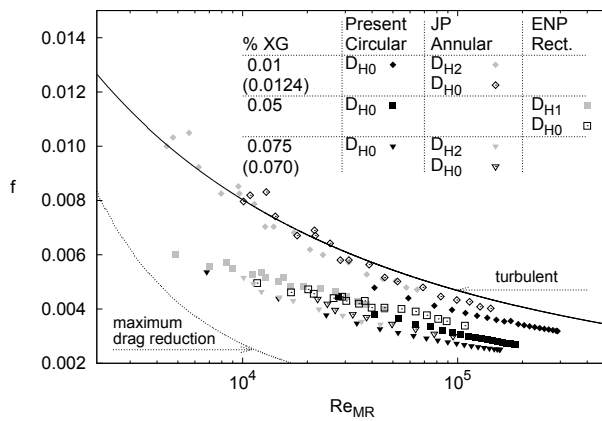
0.014

0.012

0.010

0.008

f

0.006

0.004

0.002

% XG	Present Circular	JP Annular	ENP Rect.
0.01	D_{H0} ◆	D_{H2} D_{H0} ◇	
(0.0124)			
0.05	D_{H0} ■		D_{H1} D_{H0} □
0.075	D_{H0} ▼	D_{H2} D_{H0} ▽	
(0.070)			

turbulent

maximum
drag reduction

10^4 10^5

Re_{MR}

Fig. 6.   Effect of pipe cross section: drag reduction data measured for annular [18] (JP) and rectangular [16] (ENP) section at different XG concentrations (diamonds, 0.01% XG; squares, 0.05% XG and triangles 0.075% XG); our data (solid symbols), original JP/ENP data (gray symbols) ($D_{H1} = 46\,mm, D_{H2} = 49.2\,mm$), JP/ENP data rescaled to $D_{H0} = 100\,mm$ (open symbols)
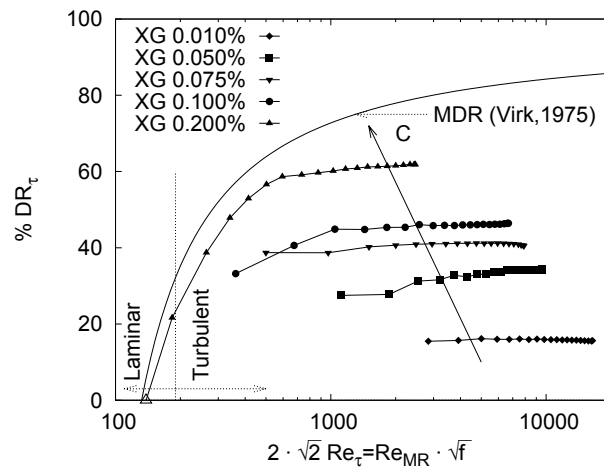
Fig. 7.   Percent drag reduction for aqueous solutions at different XG concentrations as a function of friction Reynolds number, Re_τ. Symbols represent values of XG concentration; arrow indicates increasing XG concentration; black line represents maximum drag reduction according to [31]
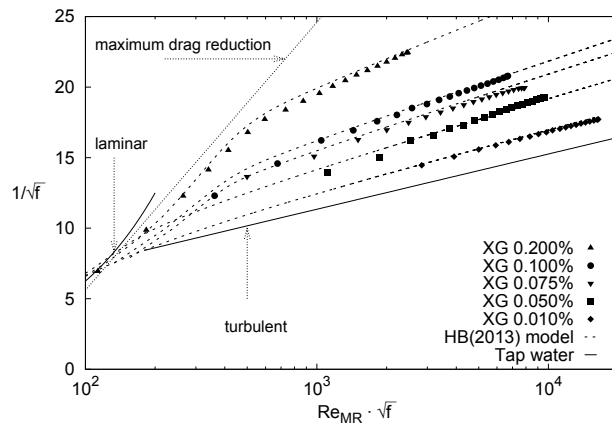
Fig. 8. Comparison between experimental data and predictive correlation by [10]: solid symbols identify data for different XG solutions; dotted lines identify Housiadas and Beris (HB2013) correlation prediction; curve for tap water (solid line) and maximum drag reduction asymptote (dotted line) are shown for reference
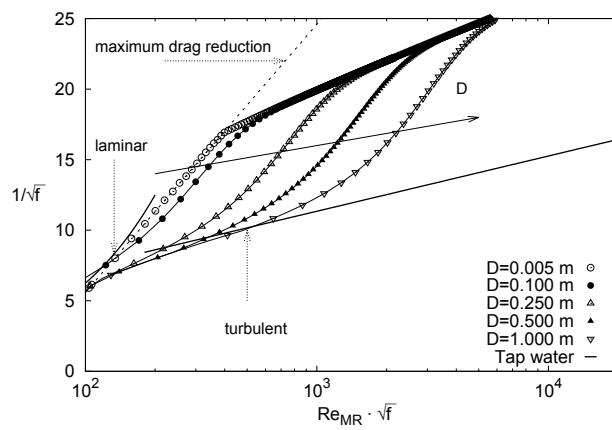
Fig. 9. Scale up and scale down of friction factor predicted by [10] correlation: curve for tap water (solid line), maximum drag reduction asymptote (dotted line), data for different pipe diameters (solid symbols)
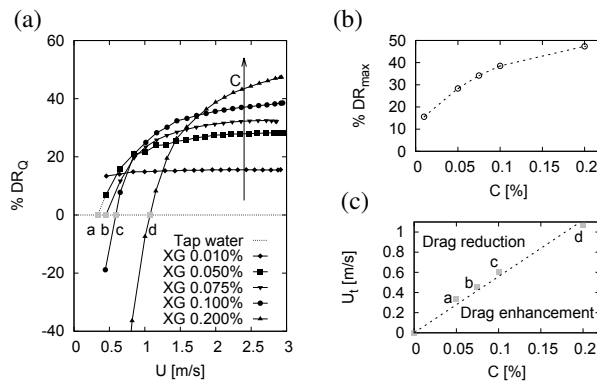
Fig. 10. (a) Percent drag reduction for aqueous solutions at different XG concentrations as a function of bulk velocity in the pipe, U. Symbols represent values of XG concentration. Arrow indicates increasing XG concentration. (b) Variation of maximum %DR, $\%DR_{max}$, as a function of XG concentration, C: the increment in %DR is less than linear with C. (c) Variation of threshold velocity for drag reduction, U_t, as a function of polymer concentration, C, and linear fit (dashed line)
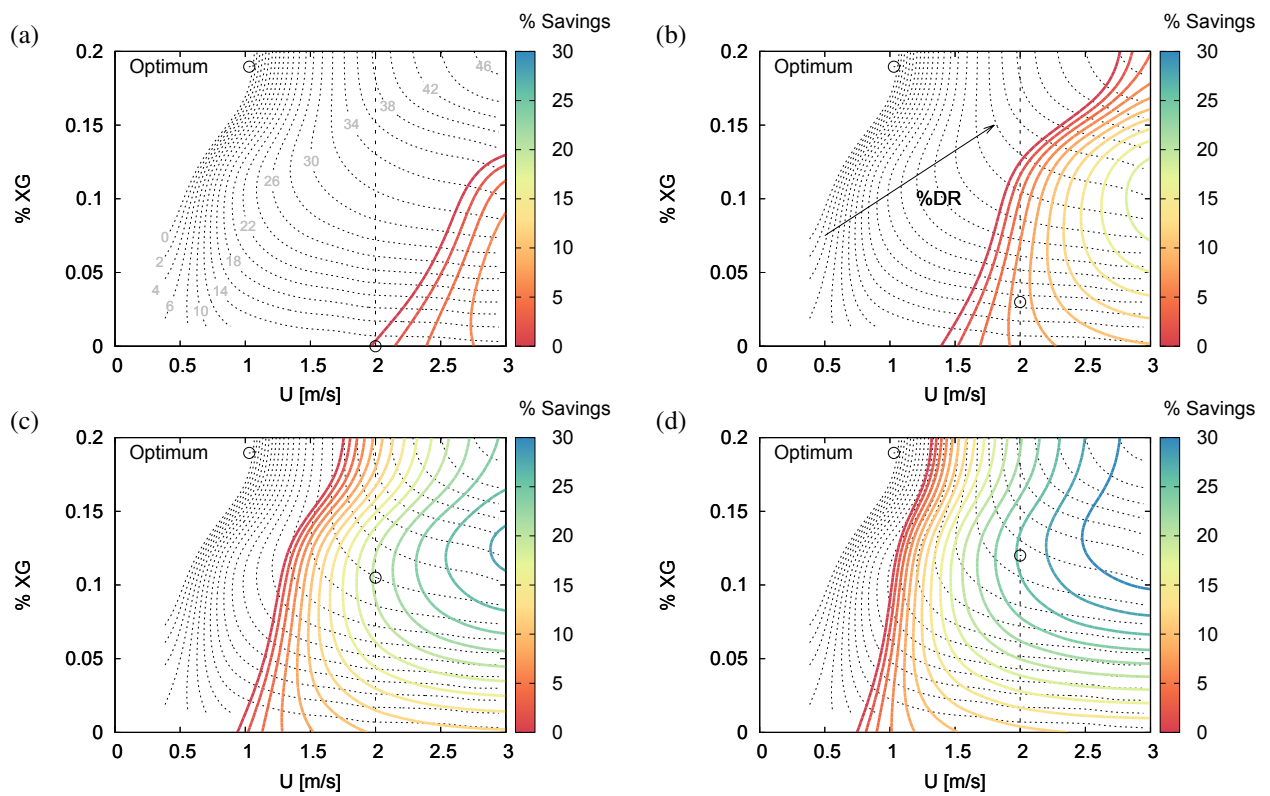
Fig. 11.   Percent net cost savings expected from use of XG as drag reducing agent: dashed lines on the background represent isocontours of $\%DR$ (starting from zero, step 2%; isocontour labels are in gray); continuous lines (in color online) represent isocontours of $\%S$ (starting from zero, step 2%); subfigures correspond to different pipeline scenario: (a) $\alpha = 5 \cdot 10^{-2} \ s^2/m^2$, (b) $\alpha = 1 \cdot 10^{-1} \ s^2/m^2$, (c) $\alpha = 2.5 \cdot 10^{-1} \ s^2/m^2$, (d) $\alpha = 5 \cdot 10^{-1} \ s^2/m^2$
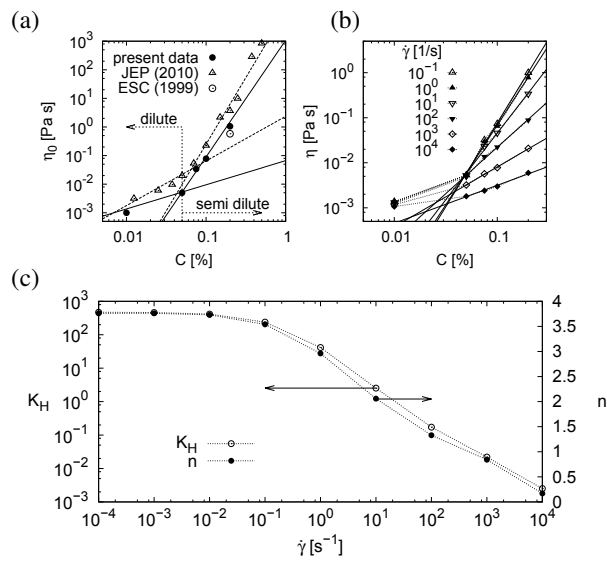
Fig. 12.   Results of rheological data processing: (a) variation of zero-shear viscosity versus concentration; present data (solid circle); ESC (1999) data [11] (open circle); JEP (2010) data [17] (open triangle); power law fitting of data in the dilute and semi-dilute concentration range (solid line, present data; dashed line, JEP data); (b) variation of viscosity versus concentration: symbols identify different values of shear rate, $\dot{\gamma}$, solid lines are power law fit, $\eta = K'_H \cdot C^{n''}$, for concentration values larger than 0.01%; (c) value of fitting parameters K'_H and n'' as a function of shear rate, $\dot{\gamma}$

Carreau-Yasuda model parameters for XG at $20^o C$					
C	η_0	η_∞	λ	a	n
$[\%]$	$[mPa \cdot s]$	$[mPa \cdot s]$	$[s]$	$[-]$	$[-]$
0.01	1.36	0.94	0.00002	0.271	1.00
0.05	5.29	1.54	0.01124	0.940	1.00
0.075	33.88	1.63	0.02454	0.437	1.00
0.1	78.45	1.65	0.21557	0.510	0.73
0.2	1062.43	1.95	3.68927	0.796	0.68
0.2[1]	578.	2.76	1.30	0.724	0.724
0.2[2]	3680.	2.24	21.5	0.81	0.66

[1] Fitting parameters from [11].

[2] Fitting parameters from [17].

Table 1. Fitting parameters of Carreau-Yasuda model for XG solutions: η_0 and η_∞ are viscosity at the zero-shear and infinite-shear plateaus, λ, n and a are inverse shear rate at onset of shear thinning, power law index and the parameter introduced by [25]

%XG	0.01	0.05	0.075	0.10	0.2
LDR	0.13	0.30	0.39	0.44	0.61

Table 2.   Value of dimensionless parameters used to assess [10] correlation. $El_0 = 0.087$ for all %XG concentrations